Science Advances
AAAS

Supplementary Materials for

Extensive programmed centriole elimination unveiled in *C. elegans* embryos

Nils Kalbfuss and Pierre Gönczy

Corresponding author: Pierre Gönczy, pierre.gonczy@epfl.ch

Sci. Adv. **9**, eadg8682 (2023)
DOI: 10.1126/sciadv.adg8682

The PDF file includes:

Other Supplementary Material for this manuscript includes the following:

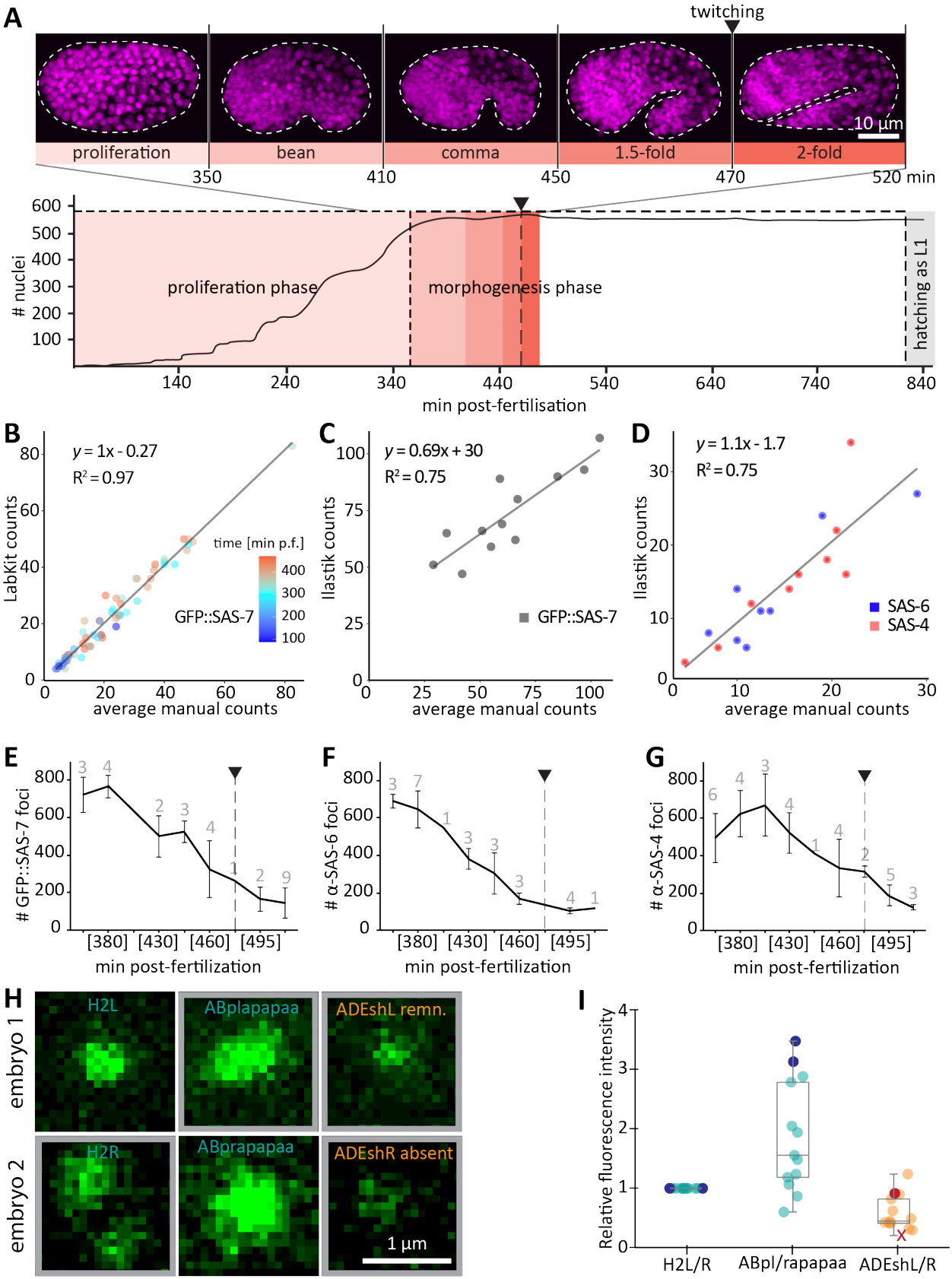
A
twitching
10 µm
proliferation
bean
comma
1.5-fold
2-fold
350
410
450
470
520 min
nuclei
proliferation phase
morphogenesis phase
hatching as L1
min post-fertilisation
B
y = 1x - 0.27
R² = 0.97
LabKit counts
time [min p.f.]
GFP::SAS-7
average manual counts
C
y = 0.69x + 30
R² = 0.75
Ilastik counts
GFP::SAS-7
average manual counts
D
y = 1.1x - 1.7
R² = 0.75
Ilastik counts
SAS-6
SAS-4
average manual counts
E
GFP::SAS-7 foci
[380] [430] [460] [495]
min post-fertilization
F
α-SAS-6 foci
[380] [430] [460] [495]
min post-fertilization
G
α-SAS-4 foci
[380] [430] [460] [495]
min post-fertilization
H
embryo 1
H2L
ABplapapaa
ADEshL remn.
embryo 2
H2R
ABprapapaa
ADEshR absent
1 µm
I
Relative fluorescence intensity
H2L/R
ABpl/rapapaa
ADEshL/R

Figure S1

Fig. S1. Assessing centriole numbers during *C. elegans* embryogenesis
(A) Timeline of *C. elegans* embryogenesis. Nuclear numbers increase during the proliferation phase and are stable during the morphogenesis phase that follows (with increasing shades of red, used throughout the manuscript), with some minor fluctuations reflecting cell division and rapid programmed cell death events (the latter pertaining to 131 cells in total). Embryo age can be estimated during morphogenesis based on the extent of elongation (bean, comma, 1.5- and 2-fold stages, as illustrated with exemplary maximum z-projections of DNA-stained embryos in magenta). Note that after the 1.5-fold stage, at ~470 min post-fertilization at 20-22 °C, the embryo starts twitching (arrowhead and vertical dashed line). Number of nuclei and timing adapted from (***12***). **(B-D)** Comparison of machine learning counts versus average manual count, performed twice for B and D, plots show average, once for C; the average difference between the two manual counts was -1 (+/- 3.6) (B) or -0.4 (+/- 2.6) (D). LabKit counts for GFP::SAS-7 foci detection in lattice light-sheet data (B, colour code indicates developmental time post-fertilization (p.f.)), Ilastik counts for GFP::SAS-7 foci detection in fixed samples (C), as well as Ilastik counts for SAS-6 and SAS-4 foci in immunostaining experiments (D). **(E-G)** Quantifications of fixed (E) or immunostained (F, G) images of GFP::SAS-7 (E), SAS-6 (F), and SAS-4 (G) foci according to approximate time post-fertilization, estimated from the stage of the imaged embryos. Averages +/- SD are shown, with the number of embryos analyzed indicated in each case. **(H)** High-magnification views illustrating GFP::SAS-7 foci intensity in a 1.5-fold stage embryo [~460 min] just before fixation for CLEM analysis. Images surrounded by a grey box indicate the examples shown in Fig. 2. Brightness and Contrast was adjusted differently for embryo 1 and 2. In embryo 1, a centriole remnant was found for ADEshL by EM (indicated by remn. in the panel). In embryo 2, no structure was found in ADEshR by EM. **(I)** Quantification of signal intensities in the indicated cells relative to H2L/R. Note that differences in GFP::SAS-7 intensities might stem from the cells being in different cell cycle stages: at this stage the seam cells H2L/R are in G1, the seam progenitor cells ABpl/rapapaa in G2, whereas ADEshL/R cells have exited the cell cycle. Dark blue and dark red disks mark cells analyzed by CLEM. The red x marks cells in which no centriolar structure was observed (n = 13). Interestingly, the cell with a potential centriole remnant (filled disc) exhibited a brighter GFP::SAS-7 focus than the average of that cell type. Note that one embryo in which no centriolar structure was detected in ADEshL/R by CLEM is not reported in this plot, because intensities in H2L/R were much lower than in the other embryos, probably due to the centriole being slightly out of focus, therefore yielding outlier values for ABpl/rapapaa (at 7) and ADEshL/R (at 1.4).

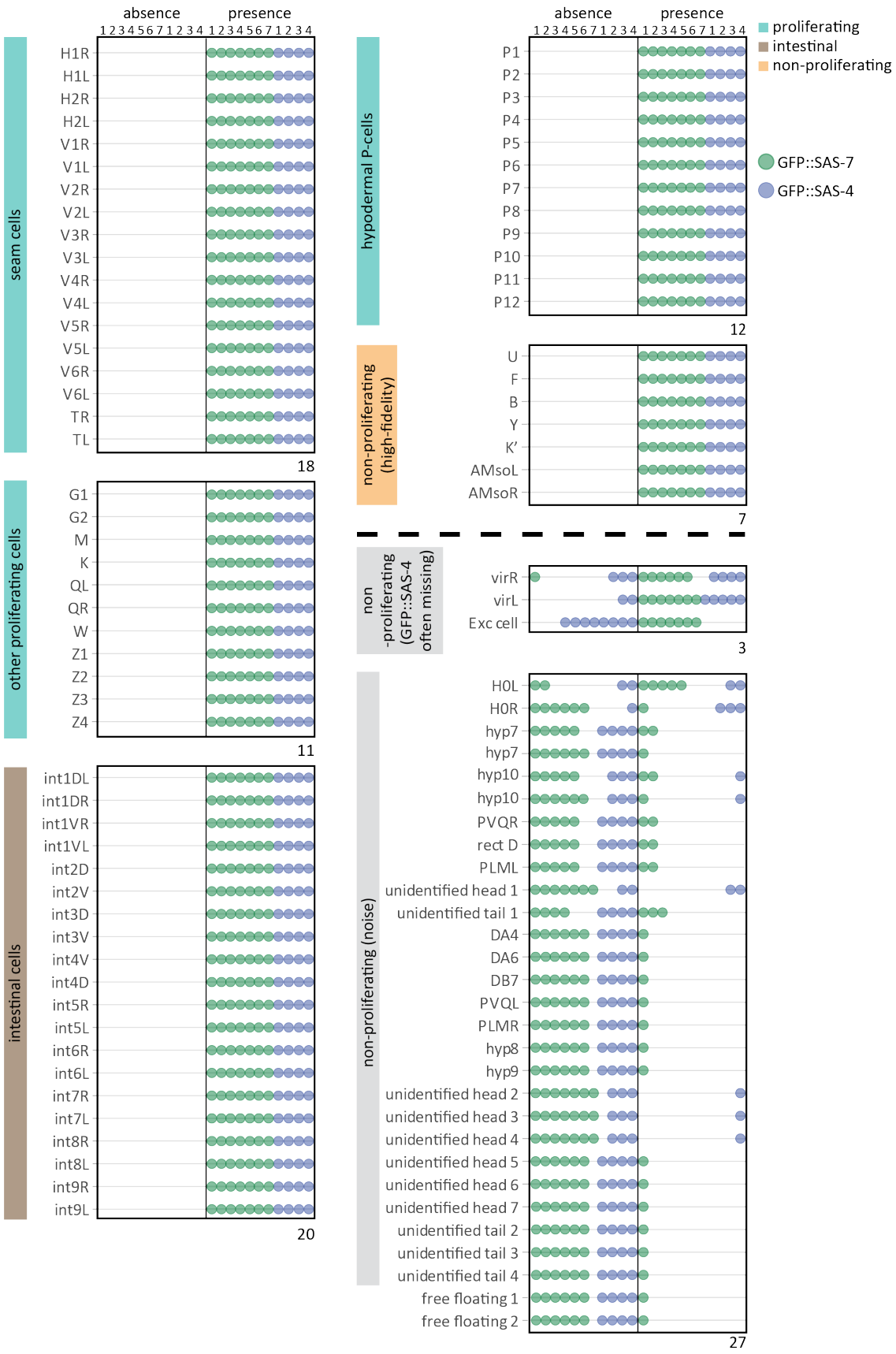
absence
presence
1 2 3 4 5 6 7 1 2 3 4 1 2 3 4 5 6 7 1 2 3 4
proliferating
intestinal
non-proliferating
GFP::SAS-7
GFP::SAS-4
seam cells
H1R
H1L
H2R
H2L
V1R
V1L
V2R
V2L
V3R
V3L
V4R
V4L
V5R
V5L
V6R
V6L
TR
TL
18
other proliferating cells
G1
G2
M
K
QL
QR
W
Z1
Z2
Z3
Z4
11
intestinal cells
int1DL
int1DR
int1VR
int1VL
int2D
int2V
int3D
int3V
int4V
int4D
int5R
int5L
int6R
int6L
int7R
int7L
int8R
int8L
int9R
int9L
20
hypodermal P-cells
P1
P2
P3
P4
P5
P6
P7
P8
P9
P10
P11
P12
12
non-proliferating (high-fidelity)
U
F
B
Y
K'
AMsoL
AMsoR
7
non -proliferating (GFP::SAS-4 often missing)
virR
virL
Exc cell
3
non-proliferating (noise)
H0L
H0R
hyp7
hyp7
hyp10
hyp10
PVQR
rect D
PLML
unidentified head 1
unidentified tail 1
DA4
DA6
DB7
PVQL
PLMR
hyp8
hyp9
unidentified head 2
unidentified head 3
unidentified head 4
unidentified head 5
unidentified head 6
unidentified head 7
unidentified tail 2
unidentified tail 3
unidentified tail 4
free floating 1
free floating 2
27

Figure S2

Fig. S2. Highly stereotyped distribution of GFP::SAS-7 and GFP::SAS-4 foci in L1 larvae
Worms expressing either GFP::SAS-7 (green) (n=7) or GFP::SAS-4 (blue) (n=4) scored for the presence or absence of foci in the indicated cells of L1 larvae; note that due to ambiguities in foci maintenance for excretory cells and vir cells, 4 additional worms were scored for these cells specifically. All proliferating (cyan) (n=41) and intestinal (brown) (n=20) cells maintained centrioles. Note that QL and QR cells had proliferated already upon scoring in two larvae, but are represented with their progenitor cells here for simplicity. Only 7 non-proliferating cells reliably maintain GFP::SAS-7 and GFP::SAS-4 foci (orange, high fidelity). In another 3 cells, GFP::SAS-4 foci are either completely absent or often missing (grey, GFP::SAS-4 often missing), whereas GFP::SAS-7 foci are usually present. In addition, in 27 more cells, a GFP::SAS-4 or GFP::SAS-7 focus was present occasionally, but this was likely noise given the low signal intensity observed in these cases (grey, noise). The number of cells within each group is indicated at the bottom right of the corresponding rectangle.

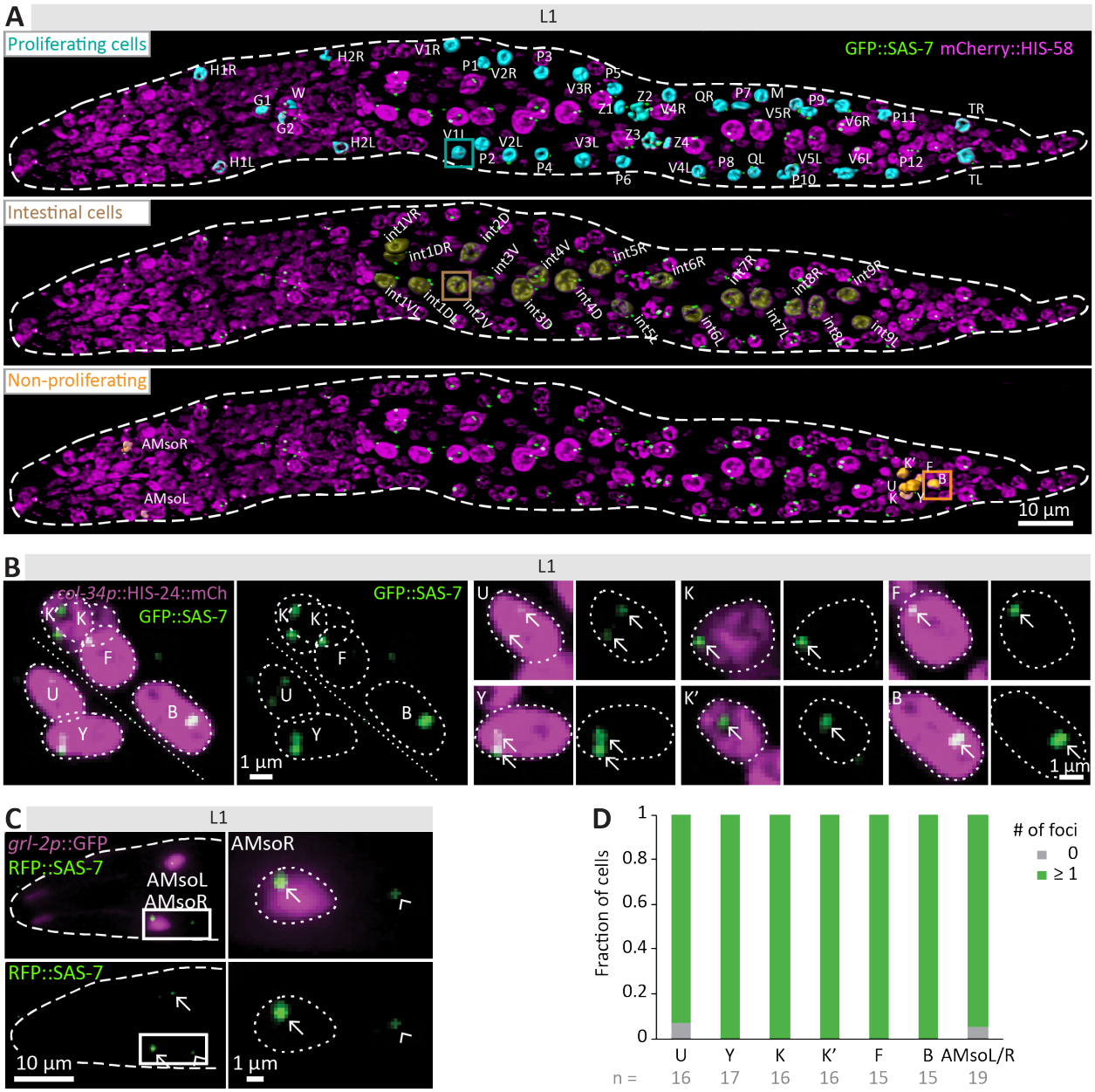
A
L1
Proliferating cells
GFP::SAS-7 mCherry::HIS-58
Intestinal cells
Non-proliferating
AMsoR
AMsoL
10 µm
B
L1
col-34p::HIS-24::mCh
GFP::SAS-7
1 µm
C
L1
grl-2p::GFP
RFP::SAS-7
AMsoL
AMsoR
10 µm
1 µm
D
Fraction of cells
# of foci
0
≥ 1
U Y K K' F B AMsoL/R
n = 16 17 16 16 15 15 19

Figure S3

Fig. S3. Verification of cell identification in non-proliferating cells with persistent foci of centriolar proteins at the L1 larval stage

(A) 3D rendition of lattice light-sheet imaging of paralyzed L1 larva expressing GFP::SAS-7 and the pan-nuclear marker mCherry::HIS-58, as well as segmentation of proliferating (cyan, top), intestinal (brown, middle) and non-proliferating (orange, bottom) cells that maintain centrioles with high fidelity overlaid. Boxes indicate cells with centrioles magnified in Figure 2B. **(B)** Confocal microscopy maximum z-projections of select planes of paralyzed L1 larva verifying GFP::SAS-7 focus maintenance in rectal epithelial cells marked by *col-34p*::HIS-24::mCherry. Arrows point to GFP::SAS-7 foci. **(C)** Maximum z-projection confocal microscopy of selected planes of paralyzed L1 larva verifying RFP::SAS-7 maintenance in AMsoL/R marked with *grl-2p*::GFP. Arrows point to RFP::SAS-7 foci associated with AMsoL/R, arrowheads to foci associated with H0. Note that the RFP::SAS-7 focus is less bright in H0 than in AMso and was sometimes even absent (see fig. S2). **(D)** Fraction of cells maintaining GFP::SAS-7 foci in rectal epithelial cells and RFP::SAS-7 in AMsoL/R. The number of cells analyzed in each case is indicated at the bottom.

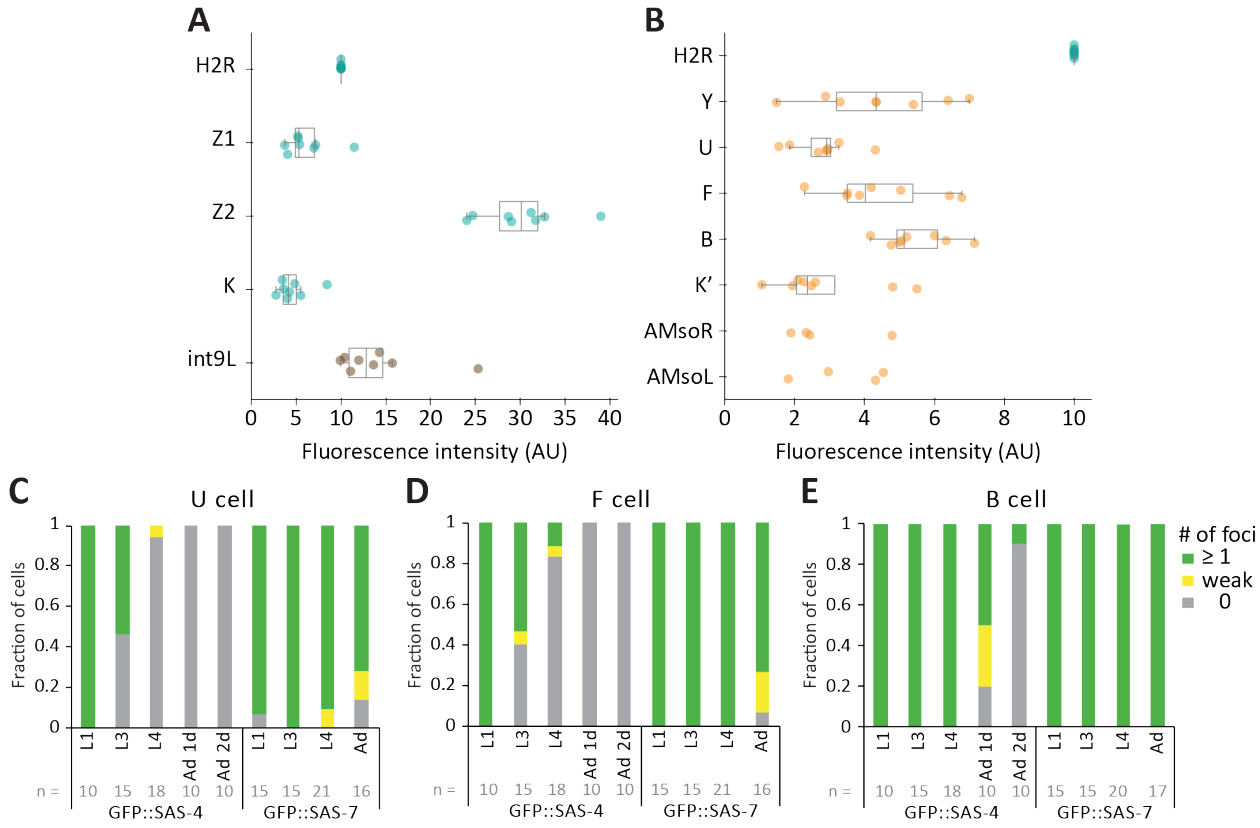
A
H2R
Z1
Z2
K
int9L
0 5 10 15 20 25 30 35 40
Fluorescence intensity (AU)
B
H2R
Y
U
F
B
K'
AMsoR
AMsoL
0 2 4 6 8 10
Fluorescence intensity (AU)
C
U cell
D
F cell
E
B cell
Fraction of cells
0 0.2 0.4 0.6 0.8 1
L1 L3 L4 Ad 1d Ad 2d L1 L3 L4 Ad
n = 10 15 18 10 10 15 15 21 16
GFP::SAS-4
GFP::SAS-7
n = 10 15 18 10 10 15 15 21 16
GFP::SAS-4
GFP::SAS-7
n = 10 15 18 10 10 15 15 20 17
GFP::SAS-4
GFP::SAS-7
# of foci
≥ 1
weak
0

Figure S4

Fig. S4. Tracking centriole fate in rectal epithelial cells through larval development and in the adult

(A, B) Quantification of GFP::SAS-7 foci fluorescence intensity relative to the average in H2R for proliferating (blue, A), intestinal (brown, A) and non-proliferating cells maintaining centrioles in L1 larvae (orange, B) (n=8). Note that the B cell, which has the highest proliferative potential in the male, has the highest intensity here. **(C-E**) Centriole fate of rectal epithelial cells during post-embryonic development. Fraction of worms without (gray), with weak (yellow) or with strong (green) foci in the indicated cell (C: U cell, D: F cell, E: B cell). *col-34p*::HIS-24::mCherry was used to identify rectal epithelial cells in the case of GFP::SAS-7, and the pan-nuclear marker mCherry::HIS-58 in the case of GFP::SAS-4. Note that GFP::SAS-4 was analyzed in adults in a *glp-4(bn2)* mutant background where germ cells, which harbor many centrioles, are essentially lacking; morphologically, these worms are healthy, with an apparently normal somatic gonad **(*63*)**. Numbers of cells analyzed at each stage are indicated below in gray. As can be seen, GFP::SAS-7 foci are maintained until adulthood in all three cases, whereas GFP::SAS-4 foci start disappearing in L3 for U and F, and in adulthood for B. Therefore, lower intensities of GFP::SAS-7 foci in the L1 stage do not reflect ongoing elimination at that stage, although they may reflect centrioles fated to be eliminated at much later stages in some cases.

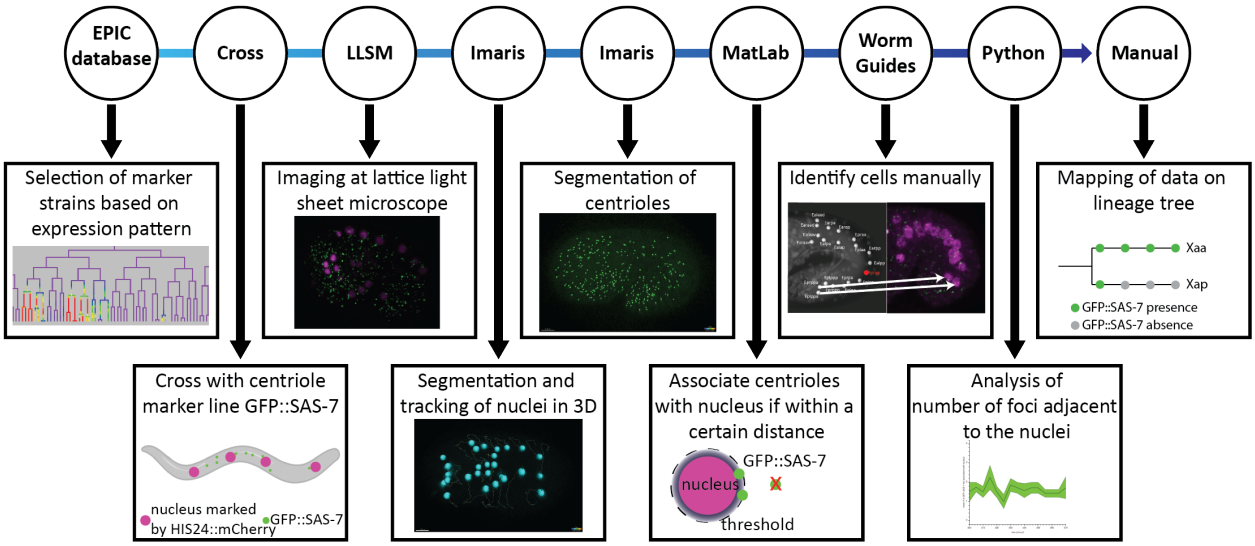
EPIC database
Cross
LLSM
Imaris
Imaris
MatLab
Worm Guides
Python
Manual
Selection of marker strains based on expression pattern
Imaging at lattice light sheet microscope
Segmentation of centrioles
Identify cells manually
Mapping of data on lineage tree
Xaa
Xap
GFP::SAS-7 presence
GFP::SAS-7 absence
Cross with centriole marker line GFP::SAS-7
nucleus marked by HIS24::mCherry
GFP::SAS-7
Segmentation and tracking of nuclei in 3D
Associate centrioles with nucleus if within a certain distance
GFP::SAS-7
nucleus
threshold
Analysis of number of foci adjacent to the nuclei

Figure S5

Fig. S5. Workflow for tracking GFP::SAS-7 foci in individual cells in the embryo
Markers for specific nuclei were selected based on their expression in the EPIC database **(*60*, *61*)** and crossed with GFP::SAS-7. Imaging was performed on the lattice light-sheet microscope. Nuclei were automatically segmented, tracked in 3D and subsequently manually corrected (see Material and Methods), before segmenting GFP::SAS-7 foci in Imaris. Using a MatLab script, GFP::SAS-7 foci were then associated to the closest nucleus if positioned within an edge-to-edge distance of 0.1 μm. Based on WormGUIDES atlas, individual nuclei were identified, as were the number of foci adjacent to the nucleus. Finally, the result was plotted manually on the lineage tree.

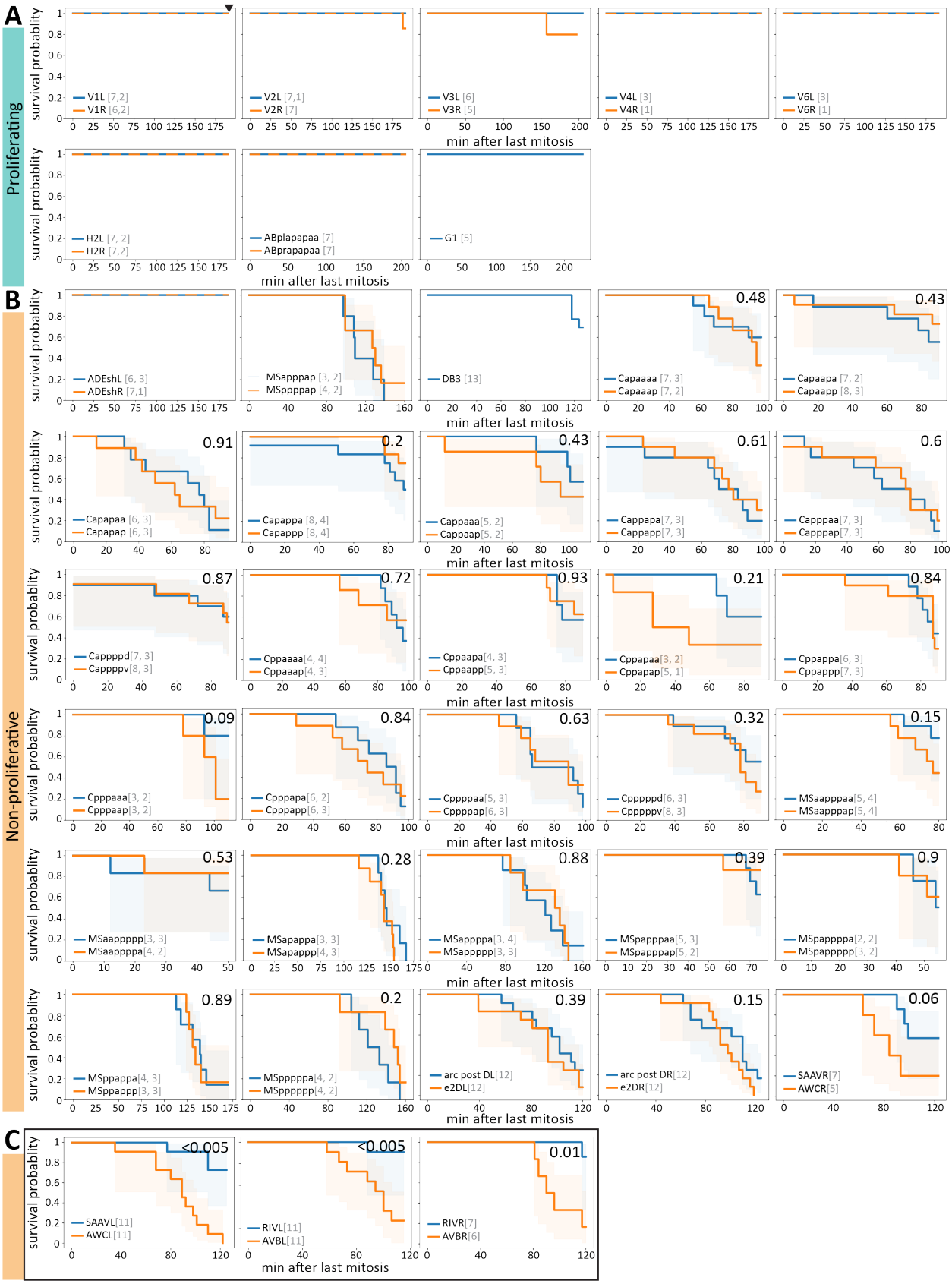
A
Proliferating
survival probablity
V1L [7,2]
V1R [6,2]
V2L [7,1]
V2R [7]
V3L [6]
V3R [5]
V4L [3]
V4R [1]
V6L [3]
V6R [1]
min after last mitosis
H2L [7, 2]
H2R [7,2]
ABplapapaa [7]
ABprapapaa [7]
G1 [5]
B
Non-proliferative
ADEshL [6, 3]
ADEshR [7,1]
MSapppap [3, 2]
MSpppppap [4, 2]
DB3 [13]
0.48
Capaaaa [7, 3]
Capaaap [7, 2]
0.43
Capaapa [7, 2]
Capaapp [8, 3]
0.91
Capapaa [6, 3]
Capapap [6, 3]
0.2
Capappa [8, 4]
Capappp [8, 4]
0.43
Cappaaa[5, 2]
Cappaap[5, 2]
0.61
Cappapa[7, 3]
Cappapp[7, 3]
0.6
Capppaa[7, 3]
Capppap[7, 3]
0.87
Cappppd[7, 3]
Cappppv[8, 3]
0.72
Cppaaaa[4, 4]
Cppaaap[4, 3]
0.93
Cppaapa[4, 3]
Cppaapp[5, 3]
0.21
Cppapaa[3, 2]
Cppapap[5, 1]
0.84
Cppappa[6, 3]
Cppappp[7, 3]
0.09
Cpppaaa[3, 2]
Cpppaap[3, 2]
0.84
Cpppapa[6, 2]
Cpppapp[6, 3]
0.63
Cppppaa[5, 3]
Cppppap[6, 3]
0.32
Cpppppd[6, 3]
Cpppppv[8, 3]
0.15
MSaapppaa[5, 4]
MSaapppap[5, 4]
0.53
MSaapppppp[3, 3]
MSaapppppa[4, 2]
0.28
MSapappa[3, 3]
MSapappp[4, 3]
0.88
MSappppa[3, 4]
MSapppppp[3, 3]
0.39
MSappppaa[5, 3]
MSappppap[5, 2]
0.9
MSappppppa[2, 2]
MSappppppp[3, 2]
0.89
MSppappa[4, 3]
MSppappp[3, 3]
0.2
MSpppppa[4, 2]
MSppppppp[4, 2]
0.39
arc post DL[12]
e2DL[12]
0.15
arc post DR[12]
e2DR[12]
0.06
SAAVR[7]
AWCR[5]
C
<0.005
SAAVL[11]
AWCL[11]
<0.005
RIVL[11]
AVBL[11]
0.01
RIVR[7]
AVBR[6]

Figure S6

Fig. S6. Kaplan-Meier curves for centriole fate of tracked nuclei

(A-C) Kaplan-Meier curves reporting the presence of GFP::SAS-7 foci adjacent to nuclei in indicated cells in minutes following the last mitosis. The dataset includes the indicated proliferating (A) and non-proliferating (B) cells. Note that the scale of the x-axis differs between plots, with the end of the x-axis always corresponding to twitching onset, thus allowing to better recognize potential differences between sister cells. 95 % confidence interval and p-values (upper right corner) of pairwise log-rank test are shown for all sister cells. If not indicated, mirror cells are shown on the same plot and neither confidence nor p-values are shown. (C) Note that in the cases of SAAVL/AWCL, RIVL/AVBL and RIVR/AVBR, the two sister cells are significantly different. The equivalent mirror cells SAAVR/AWCR also exhibits a low p-value, although just below significance probably due to low numbers (see B). AWCR/L are sensory neurons where centrioles migrate away from the nucleus before templating sensory cilia **(*22*)**. The number of cells analysed is indicated in gray in each case. If two values are provided, the first number indicates the number of cells analyzed in 3 min interval movies, the second the number of cells analyzed in 1 min interval movies. Note that centrioles appeared to be missing in rare proliferating cells (in V2R and V3R) just before twitching, likely because of technical reasons since GFP::SAS-7 foci are invariably present in L1 larvae in these cells.

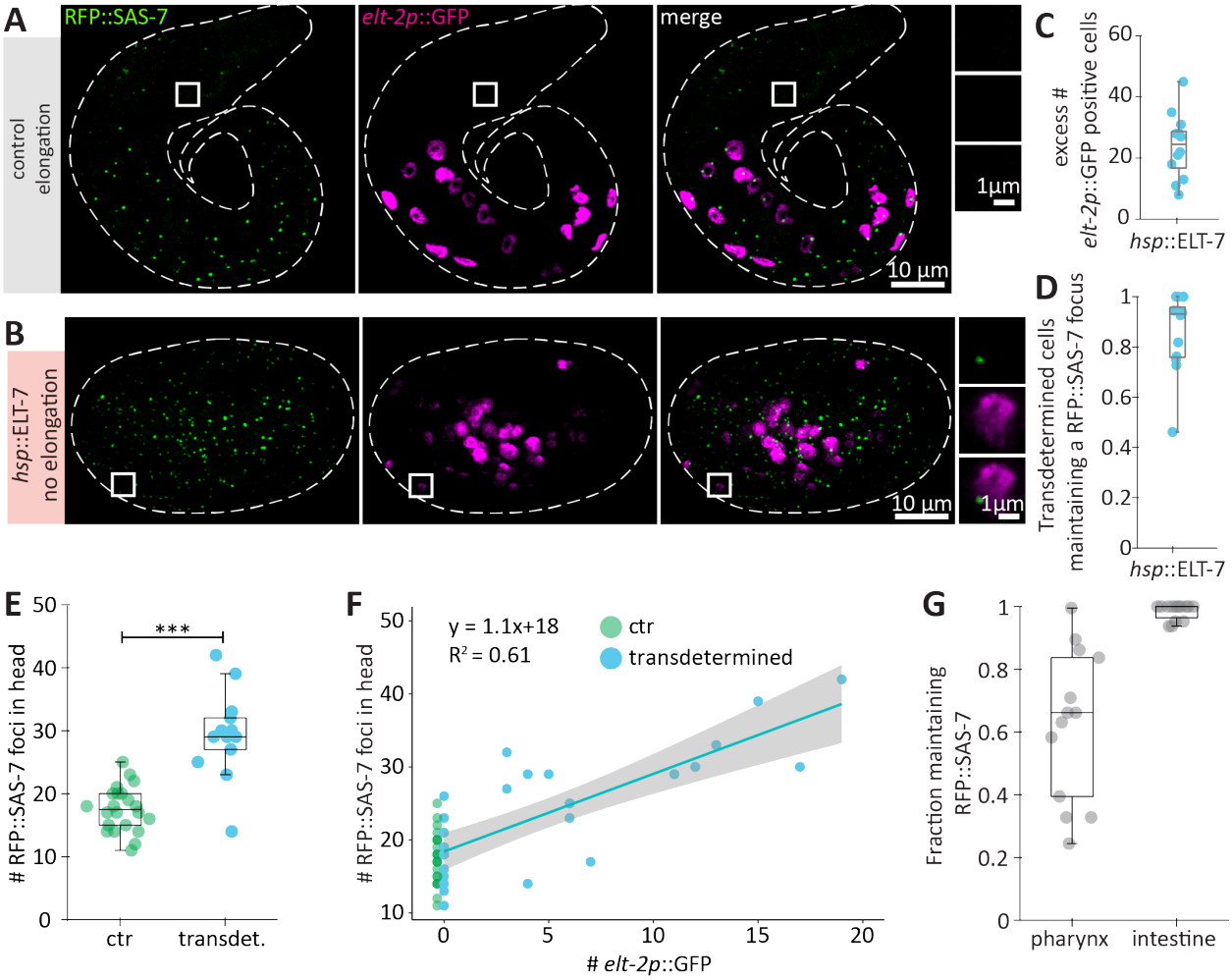
A
RFP::SAS-7
elt-2p::GFP
merge
control elongation
1µm
10 µm
B
hsp::ELT-7 no elongation
10 µm
1µm
C
excess # elt-2p::GFP positive cells
hsp::ELT-7
D
Transdetermined cells maintaining a RFP::SAS-7 focus
hsp::ELT-7
E
RFP::SAS-7 foci in head
***
ctr
transdet.
F
y = 1.1x+18
R² = 0.61
ctr
transdetermined
RFP::SAS-7 foci in head
elt-2p::GFP
G
Fraction maintaining RFP::SAS-7
pharynx
intestine

Figure S7

Fig. S7. Further analysis of transdetermination experiments imparted by excess ELT-7
(A, B) Maximum z-projections of live wide-field microscopy of embryos that were heat-shocked prior to overnight incubation; embryos express RFP::SAS-7 and the intestine-specific marker *elt-2p*::GFP (A), plus ELT-7 under a heat-shock promoter (denoted *hsp*::ELT-7 to abbreviate *hsp16-2/41p*::ELT-7) (B). Control embryos hatched as L1 (n=6/6) (A). After global heat-shock leading to ELT-7 overexpression in embryos of the proliferation phase (B), embryos arrested and did not go through morphogenesis (n =11/11). Boxes indicate areas highlighted in insets with z-projection of the planes where only the nucleus is located. **(C)** Number of excess *elt-2p*::GFP positive nuclei detected after heat-shock. In the wild-type, 20 *elt-2p*::GFP cells are expected; this number was subtracted in each case to obtain the excess number of intestinal cells. **(D)** Fraction of excess *elt-2p*::GFP positive cells maintaining RFP::SAS-7 foci. Note that although ELT-7 overexpression before morphogenesis led to embryonic arrest, most supernumerary *elt-2p*::GFP positive cells harbored RFP::SAS-7 foci. **(E)** Quantification of RFP::SAS-7 foci in head region of control and locally transdetermined cells. Significance as computed by Welch test. P-value = $8.17*10^{-5}$. **(F)** Plot of overall RFP::SAS-7 foci number in head region as a function of *elt-2p*::GFP positive cells in the pharynx for control (green) and transdetermined (blue) animals. A linear model is shown with 95 % confidence interval in gray. **(G)** Fraction of pharyngeal versus intestinal cells expressing *elt-2p*::GFP and maintaining centrioles after local transdetermination of pharyngeal cells. Note that the two larvae with the highest fraction of transdetermined cells maintaining RFP::SAS-7 were also the two youngest locally heat-shocked embryos that still managed to hatch. Late overexpression of ELT-7 when centrioles are already eliminated does not lead to reappearance of RFP::SAS-7 foci. In control conditions, ~3% of cells in the head maintain RFP::SAS-7 foci.

Lab designation	Genotype	References
Centriole elimination in embryo and L1		
GZ1663	*sas-7(or1940[gfp::sas-7])III; bqSi189[pBN13(unc-119(+) Plmn-1::mCherry::his-58)] II; glo-1(zu931)X, may carry unc-119(ed9) III*	(*46*, *64*)
GZ1854	*sas-4(bs195[gfp::sas-4] III, glo-1(zu931)X, bqSi189[pBN13(unc-119(+) Plmn-1::mCherry::his-58)] II*	(*64*) GFP::SAS-4 is a gift from Kevin O'Connell;
GZ1848	*sas-7(is1[rfp::sas-7+loxP])III; glo-1(zu931)X wIs54 [scm::GFP] V*	(*65*, *66*)
GZ1866 (expression of *grl-2p*::GFP)	*dpy-5(e907) I; sEx12852[rCesT16G1.8::GFP + pCeh361], sas-7(is1[rfp::sas-7+loxP])III, glo-1(zu931)X;*	(*66*, *67*)
GZ1808	*stIs10661 [ceh-16.b::H1-Wcherry::his-24::mCherry + unc-119(+)]II; glo-1(zu931)X; pcmd-1(syb486[gfp::pcmd-1]) I*	(*61*, *68*)
Embryo Lineaging		
GZ1731	*stIs10661 [ceh-16.b::H1-Wcherry::his-24::mCherry + unc-119(+)]; sas-7(or1940[gfp::sas-7])III; glo-1(zu931)X*	(*46*, *61*)
GZ1754	*stIs10544 [hlh-16::H1-wCherry::let-858 3' UTR], sas-7(or1940[gfp::sas-7])III, glo-1(zu931)X*	(*46*, *61*)
GZ1692	*stIs10088 [hlh-1(3.3kb)::HIS-24::mCherry + unc-119(+)]II, sas-7(or1940[gfp::sas-7])III ; glo-1(zu931)X*	(*46*, *61*)

Transdifferentiation/transdetermination		
GZ1840	*sas-7(is1[rfp::sas-7+loxP])III, wIs125[hsp-16-2::elt-7 hsp-16-41::elt-7]; rrIs1 [elt-2::GFP + unc-119(+)], glo-1(zu931)X;*	(*66*, *69*)
GZ1841	*sas-7(is1[rfp::sas-7+loxP])III, rrIs1 [elt-2::GFP + unc-119(+)]; glo-1(zu931)X;*	(*66*, *69*)
GZ1927	*sas-7(or1940[gfp::sas-7])III; glo-1(zu931)X, gaIs245[col-34p::HIS-24::mCherry; unc-119(+)] V;*	(*46*, *70*)
GZ1868	*syIs63 [cog-1::GFP + unc-119(+)], sas-7(is1[rfp::sas-7+loxP])III, glo-1(zu931)X*	(*66*, *71*)
GZ1945	*sem-4(n1971)I, sas-7(or1940[gfp::sas-7])III, glo-1(zu931)X, gaIs245[col-34p::HIS-24::mCherry; unc-119(+)] V;*	(*46*, *70*, *72*)

Table S1. Strains used in this study.

Movie S1. Movie from dual-color time-lapse lattice light-sheet microscopy showing embryo expressing GFP::SAS-7 and HIS-58::mCherry. Corresponding still images are shown in Figure 1A. Time indicates minutes after fertilization. The timepoint of twitching was set to 470 min post-fertilization.

REFERENCES AND NOTES

1. P. Gönczy, G. N. Hatzopoulos, Centriole assembly at a glance. *J. Cell Sci.* **132**, jcs228833 (2019).

2. L. Pintard, B. Bowerman, Mitotic Cell Division in *Caenorhabditis elegans*. *Genetics* **211**, 35–73 (2019).

3. Z. Carvalho-Santos, J. Azimzadeh, J. B. Pereira-Leal, M. Bettencourt-Dias, Tracing the origins of centrioles, cilia, and flagella. *J. Cell Biol.* **194**, 165–175 (2011).

4. M. G. Riparbelli, V. Persico, M. Gottardo, The developing *Drosophila* eye: An oncoming model to study centriole reduction, (2018).

5. A. M. Tassin, B. Maro, M. Bornens, Fate of microtubule-organizing centers during myogenesis in vitro. *J. Cell Biol.* **100**, 35–46 (1985).

6. E. Bugnard, K. J. M. Zaal, E. Ralston, Reorganization of microtubule nucleation during muscle differentiation. *Cell Motil. Cytoskeleton* **60**, 1–13 (2005).

7. A. P. Mahowald, J. M. Strassheim, Intercellular migration of centrioles in the germarium of *Drosophila melanogaster*. *J. Cell Biol.* **45**, 306–320 (1970).

8. A. P. Mahowald, J. H. Caulton, M. K. Edwards, A. D. Floyd, Loss of centrioles and polyploidization in follicle cells of *Drosophila melanogaster*. *Exp. Cell Res.* **118**, 404–410 (1979).

9. K. P. Schoenfelder, R. A. Montague, S. V. Paramore, A. L. Lennox, A. P. Mahowald, D. T. Fox, Indispensable pre-mitotic endocycles promote aneuploidy in the *Drosophila* rectum. *Development* **141**, 3551–3560 (2014).

10. Y. Zheng, R. A. Buchwalter, C. Zheng, E. M. Wight, J. V. Chen, T. L. Megraw, A perinuclear microtubule-organizing centre controls nuclear positioning and basement membrane secretion. *Nat. Cell Biol.* **22**, 297–309 (2020).

11. J. E. Sulston, H. R. Horvitz, Post-embryonic cell lineages of the nematode, *Caenorhabditis elegans*. *Dev. Biol.* **56**, 110–156 (1977).

12. J. E. Sulston, E. Schierenberg, J. G. White, J. N. Thomson, The embryonic cell lineage of the nematode *Caenorhabditis elegans*. *Dev. Biol.* **100**, 64–119 (1983).

13. M. Ohta, A. Desai, K. Oegema, How centrioles acquire the ability to reproduce. *eLife* **6**, e25358 (2017).

14. A. Woglar, M. Pierron, F. Z. Schneider, K. Jha, C. Busso, P. Gönczy, Molecular architecture of the *C. elegans* centriole. *PLOS Biol.* **20**, e3001784 (2022).

15. F. R. Balestra, L. Von Tobel, P. Gönczy, Paternally contributed centrioles exhibit exceptional persistence in *C. elegans* embryos. *Cell Res.* **25**, 642–644 (2015).

16. M. Kirkham, T. Müller-Reichert, K. Oegema, S. Grill, A. A. Hyman, SAS-4 is a *C. elegans* centriolar protein that controls centrosome size. *Cell* **112**, 575–587 (2003).

17. S. Leidel, P. Gönczy, SAS-4 is essential for centrosome duplication in *C. elegans* and is recruited to daughter centrioles once per cell cycle. *Dev. Cell* **4**, 431–439 (2003).

18. S. Leidel, M. Delattre, L. Cerutti, K. Baumer, P. Gönczy, SAS-6 defines a protein family required for centrosome duplication in *C. elegans* and in human cells. *Nat. Cell Biol.* **7**, 115–125 (2005).

19. A. Dammermann, T. Müller-Reichert, L. Pelletier, B. Habermann, A. Desai, K. Oegema, Centriole assembly requires both centriolar and pericentriolar material proteins. *Dev. Cell* **7**, 815–829 (2004).

20. P. N. Inglis, G. Ou, M. R. Leroux, J. M. Scholey, The sensory cilia of *Caenorhabditis elegans*. *WormBook* 10.1895/wormbook.1.126.2 1–22 (2007).

21. D. Serwas, T. Y. Su, M. Roessler, S. Wang, A. Dammermann, Centrioles initiate cilia assembly but are dispensable for maturation and maintenance in *C. elegans*. *J. Cell Biol.* **216**, 1659–1671 (2017).

22. W. Li, P. Yi, Z. Zhu, X. Zhang, W. Li, G. Ou, Centriole translocation and degeneration during ciliogenesis in *Caenorhabditis elegans* neurons. *EMBO J.* **36**, 2553–2566 (2017).

23. Y. Lu, R. Roy, Centrosome/cell cycle uncoupling and elimination in the endoreduplicating intestinal cells of *C. elegans*. *PLOS ONE* **9**, e110958 (2014).

24. M.-K. Wong, V. W. S. Ho, L. Chan, R. Li, X. Ren, Z. Zhao, *Gap Phase Introduction in Every Cell Cycle of C. Elegans Embryogenesis* (CellPress Sneak Peek, 2018).

25. B.-C. Chen, W. R. Legant, K. Wang, L. Shao, D. E. Milkie, M. W. Davidson, C. Janetopoulos, X. S. Wu, J. A. Hammer 3rd, Z. Liu, B. P. English, Y. Mimori-Kiyosue, D. P. Romero, A. T. Ritter, J. Lippincott-Schwartz, L. Fritz-Laylin, R. D. Mullins, D. M. Mitchell, J. N. Bembenek, A.-C. Reymann, R. Böhme, S. W. Grill, J. T. Wang, G. Seydoux, U. S. Tulu, D. P. Kiehart, E. Betzig, Lattice light-sheet microscopy: Imaging molecules to embryos at high spatiotemporal resolution. *Science* **346**, 1257998 (2014).

26. F. Long, H. Peng, X. Liu, S. K. Kim, E. Myers, A 3D digital atlas of *C. elegans* and its application to single-cell analyses. *Nat. Methods* **6**, 667–672 (2009).

27. K. F. O'Connell, C. Caron, K. R. Kopish, D. D. Hurd, K. J. Kemphues, Y. Li, J. G. White, The *C. elegans* zyg-1 gene encodes a regulator of centrosome duplication with distinct maternal and paternal roles in the embryo. *Cell* **105**, 547–558 (2001).

28. B. A. Edgar, N. Zielke, C. Gutierrez, Endocycles: A recurrent evolutionary innovation for post-mitotic cell growth. *Nat. Rev. Mol. Cell Biol.* **15**, 197–210 (2014).

29. Z. F. Altun, D. H. Hall, *WormAtlas Hermaphrodite Handbook –Alimentary System– Intestine* (WormAtlas, 2009).

30. M. Sammut, S. J. Cook, K. C. Q. Nguyen, T. Felton, D. H. Hall, S. W. Emmons, R. J. Poole, A. Barrios, Glia-derived neurons are required for sex-specific learning in *C. elegans*. *Nature* **526**, 385–390 (2015).

31. M. R. Riddle, A. Weintraub, K. C. Q. Nguyen, D. H. Hall, J. H. Rothman, Transdifferentiation and remodeling of post-embryonic *C. elegans* cells by a single transcription factor. *Development* **140**, 4844–4849 (2013).

32. J. G. White, E. Southgate, J. N. Thomson, S. Brenner, The structure of the nervous system of the nematode *Caenorhabditis elegans*. *Philos. Trans. R. Soc. Lond. B Biol. Sci.* **314**, 1–340 (1986).

33. S. Jarriault, Y. Schwab, I. Greenwald, A *Caenorhabditis elegans* model for epithelial–neuronal transdifferentiation. *Proc. Natl. Acad. Sci. U.S.A.* **105**, 3790–3795 (2008).

34. G. Manandhar, H. Schatten, P. Sutovsky, Centrosome reduction during gametogenesis and its significance. *Biol. Reprod.* **72**, 2–13 (2005).

35. T. Boveri, *Zellen-Studien: Ueber die Natur der Centrosomen* (G. Fischer, 1900).

36. G. Schatten, The centrosome and its mode of inheritance: The reduction of the centrosome during gametogenesis and its restoration during fertilization. *Dev. Biol.* **165**, 299–335 (1994).

37. M. Delattre, P. Gönczy, The arithmetic of centrosome biogenesis, *J. Cell Sci.* **117**, 1619–1630 (2004).

38. A. H. Sathananthan, K. Selvaraj, M. L. Girijashankar, V. Ganesh, P. Selvaraj, A. O. Trounson, From oogonia to mature oocytes: Inactivation of the maternal centrosome in humans. *Microsc. Res. Tech.* **69**, 396–407 (2006).

39. A. Pimenta-Marques, I. Bento, C. A. M. Lopes, P. Duarte, S. C. Jana, M. Bettencourt-Dias, A mechanism for the elimination of the female gamete centrosome in *Drosophila melanogaster*. *Science* **353**, aaf4866 (2016).

40. M. Pierron, N. Kalbfuss, J. Borrego-pinto, P. Lénárt, P. Gönczy, Centriole foci persist in starfish oocytes despite Polo-like kinase 1 inactivation or loss of microtubule nucleation activity. *Mol. Biol. Cell* **31**, 873–880 (2020).

41. J. Magescas, S. Eskinazi, M. V. Tran, J. L. Feldman, Centriole-less pericentriolar material serves as a microtubule organizing center at the base of *C. elegans* sensory cilia. *Curr. Biol.* **31**, 2410–2417.e6 (2021).

42. J. Garbrecht, T. Laos, E. Holzer, M. Dillinger, A. Dammermann, An acentriolar centrosome at the *C. elegans* ciliary base. *Curr. Biol.* **31**, 2418–2428.e8 (2021).

43. M. Bornens, The centrosome in cells and organisms. *Science* **335**, 422–426 (2012).

44. E. T. O'Toole, T. H. Giddings, J. R. McIntosh, S. K. Dutcher, Three-dimensional organization of basal bodies from wild-type and δ-tubulin deletion strains of Chlamydomonas reinhardtii. *Mol. Biol. Cell* **14**, 2999–3012 (2003).

45. L. Pelletier, E. O'Toole, A. Schwager, A. A. Hyman, T. Müller-Reichert, Centriole assembly in *Caenorhabditis elegans*. *Nature* **444**, 619–623 (2006).

46. K. Sugioka, D. R. Hamill, J. B. Lowry, M. E. McNeely, M. Enrick, A. C. Richter, L. E. Kiebler, J. R. Priess, B. Bowerman, Centriolar SAS-7 acts upstream of SPD-2 to regulate centriole assembly and pericentriolar material formation. *eLife* **6**, e20353 (2017).

47. J. T. Wang, D. Kong, C. R. Hoerner, J. Loncarek, T. Stearns, Centriole triplet microtubules are required for stable centriole formation and inheritance in human cells. *eLife* **6**, e29061 (2017).

48. A. Bezler, P. Gönczy, Mutual antagonism between the anaphase promoting complex and the spindle assembly checkpoint contributes to mitotic timing in *Caenorhabditis elegans*. *Genetics* **186**, 1271–1283 (2010).

49. Y. L. Wong, J. V. Anzola, R. L. Davis, M. Yoon, A. Motamedi, A. Kroll, C. P. Seo, J. E. Hsia, S. K. Kim, J. W. Mitchell, B. J. Mitchell, A. Desai, T. C. Gahman, A. K. Shiau, K.

Oegema, Reversible centriole depletion with an inhibitor of Polo-like kinase 4. *Science* **348**, 1155–1160 (2015).

50. A. Khodjakov, C. L. Rieder, Centrosomes enhance the fidelity of cytokinesis in vertebrates and are required for cell cycle progression. *J. Cell Biol.* **153**, 237–242 (2001).

51. R. Basto, J. Lau, T. Vinogradova, A. Gardiol, C. G. Woods, A. Khodjakov, J. W. Raff, Flies without Centrioles. *Cell* **125**, 1375–1386 (2006).

52. S. Elmore, Apoptosis: A review of programmed cell death. *Toxicol. Pathol.* **35**, 495–516 (2007).

53. S. Brenner, The genetics of *Caenorhabditis elegans*. *Genetics* **77**, 71–94 (1974).

54. T.-L. Liu, S. Upadhyayula, D. E. Milkie, V. Singh, K. Wang, I. A. Swinburne, K. R. Mosaliganti, Z. M. Collins, T. W. Hiscock, J. Shea, A. Q. Kohrman, T. N. Medwig, D. Dambournet, R. Forster, B. Cunniff, Y. Ruan, H. Yashiro, S. Scholpp, E. M. Meyerowitz, D. Hockemeyer, D. G. Drubin, B. L. Martin, D. Q. Matus, M. Koyama, S. G. Megason, T. Kirchhausen, E. Betzig, Observing the cell in its native state: Imaging subcellular dynamics in multicellular organisms. *Science* **360**, eaaq1392 (2018).

55. A. D. Edelstein, M. A. Tsuchida, N. Amodaj, H. Pinkard, R. D. Vale, N. Stuurman, Advanced methods of microscope control using μManager software. *J. Biol. Methods* **1**, e10 (2014).

56. R. V. Aroian, C. Field, G. Pruliere, C. Kenyon, B. M. Alberts, Isolation of actin-associated proteins from *Caenorhabditis elegans* oocytes and their localization in the early embryo. *EMBO J.* **16**, 1541–1549 (1997).

57. M. Delattre, S. Leidel, K. Wani, K. Baumer, J. Bamat, H. Schnabel, R. Feichtinger, R. Schnabel, P. Gönczy, Centriolar SAS-5 is required for centrosome duplication in *C. elegans*. *Nat. Cell Biol.* **6**, 656–664 (2004).

58. M. Arzt, J. Deschamps, C. Schmied, T. Pietzsch, D. Schmidt, P. Tomancak, R. Haase, F. Jug, LABKIT: Labeling and segmentation toolkit for big image data. *Front. Comput. Sci.* **4**, 10.3389/fcomp.2022.777728 (2022).

59. S. Berg, D. Kutra, T. Kroeger, C. N. Straehle, B. X. Kausler, C. Haubold, M. Schiegg, J. Ales, T. Beier, M. Rudy, K. Eren, J. I. Cervantes, B. Xu, F. Beuttenmueller, A. Wolny, C. Zhang, U. Koethe, F. A. Hamprecht, A. Kreshuk, ilastik: Interactive machine learning for (bio)image analysis. *Nat. Methods* **16**, 1226–1232 (2019).

60. D. L. Mace, P. Weisdepp, L. Gevirtzman, T. Boyle, R. H. Waterston, A high-fidelity cell lineage tracing method for obtaining systematic spatiotemporal gene expression patterns in *Caenorhabditis elegans*. *G3: Genes Genomes Genet.* **3**, 851–863 (2013).

61. J. I. Murray, T. J. Boyle, E. Preston, D. Vafeados, B. Mericle, P. Weisdepp, Z. Zhao, Z. Bao, M. Boeck, R. H. Waterston, Multidimensional regulation of gene expression in the *C. elegans* embryo. *Genome Res.* **22**, 1282–1294 (2012).

62. A. Santella, R. Catena, I. Kovacevic, P. Shah, Z. Yu, J. Marquina-solis, A. Kumar, Y. Wu, J. Schaff, D. Colón-ramos, H. Shroff, W. A. Mohler, Z. Bao, WormGUIDES: An interactive single cell developmental atlas and tool for collaborative multidimensional data exploration. *BMC Bioinformatics* **16**, 189 (2015).

63. M. J. Beanan, S. Strome, Characterization of a germ-line proliferation mutation in *C. elegans*. *Development* **116**, 755–766 (1992).

64. G. Gómez-Saldivar, A. Fernandez, Y. Hirano, M. Mauro, A. Lai, C. Ayuso, T. Haraguchi, Y. Hiraoka, F. Piano, P. Askjaer, Identification of conserved MEL-28/ELYS domains with essential roles in nuclear assembly and chromosome segregation. *PLOS Genet.* **12**, e1006131 (2016).

65. K. Koh, J. H. Rothman, ELT-5 and ELT-6 are required continuously to regulate epidermal seam cell differentiation and cell fusion in *C. elegans*. *Development* **128**, 2867–2880 (2001).

66. K. Klinkert, N. Levernier, P. Gross, C. Gentili, L. von Tobel, M. Pierron, C. Busso, S. Herrman, S. W. Grill, K. Kruse, P. Gönczy, Aurora A depletion reveals centrosome-independent polarization mechanism in *Caenorhabditis elegans*. *eLife* **8**, e44552 (2019).

67. S. J. McKay, R. Johnsen, J. Khattra, J. Asano, D. L. Baillie, S. Chan, N. Dube, L. Fang, B. Goszczynski, E. Ha, E. Halfnight, R. Hollebakken, P. Huang, K. Hung, V. Jensen, S. J. M. Jones, H. Kai, D. Li, A. Mah, M. Marra, J. McGhee, R. Newbury, A. Pouzyrev, D. L. Riddle, E. Sonnhammer, H. Tian, D. Tu, J. R. Tyson, G. Vatcher, A. Warner, K. Wong, Z. Zhao, D. G. Moerman, Gene expression profiling of cells, tissues, and developmental stages of the nematode *C. elegans*. *Cold Spring Harb. Symp. Quant. Biol.* **68**, 159–170 (2003).

68. A. C. Erpf, L. Stenzel, N. Memar, M. Antoniolli, M. Osepashvili, R. Schnabel, B. Conradt, T. Mikeladze-Dvali, PCMD-1 organizes centrosome matrix assembly in *C. elegans*. *Curr. Biol.* **29**, 1324–1336.e6 (2019).

69. E. M. Sommermann, K. R. Strohmaier, M. F. Maduro, J. H. Rothman, Endoderm development in *Caenorhabditis elegans*: The synergistic action of ELT-2 and -7 mediates the specification→differentiation transition. *Dev. Biol.* **347**, 154–166 (2010).

70. K. Kagias, A. Ahier, N. Fischer, S. Jarriault, Members of the NODE (Nanog and Oct4-associated deacetylase) complex and SOX-2 promote the initiation of a natural cellular reprogramming event in vivo. *Proc. Natl. Acad. Sci. U.S.A.* **109**, 6596–6601 (2012).

71. R. E. Palmer, T. Inoue, D. R. Sherwood, L. I. Jiang, P. W. Sternberg, *Caenorhabditis elegans* cog-1 locus encodes GTX/Nkx6.1 homeodomain proteins and regulates multiple aspects of reproductive system development. *Dev. Biol.* **252**, 202–213 (2002).

72. M. Basson, H. R. Horvitz, The *Caenorhabditis elegans* gene sem-4 controls neuronal and mesodermal cell development and encodes a zinc finger protein. *Genes Dev.* **10**, 1953–1965 (1996).